Journal Name

ARTICLE

# Chiroptical Methods in a Wide Wavelength Range for Seeking $Ln^{3+}$ Complexes with Circularly Polarized Luminescence of Practical Interest

Received 00th January 2018,
Accepted 00th January 2018

DOI: 10.1039/x0xx00000x

www.rsc.org/

Marcin Górecki,[a,b] Luca Carpita[a], Lorenzo Arrico[a], Francesco Zinna[a] and Lorenzo Di Bari[a]*

We studied enantiopure chiral trivalent lanthanide ($Ln^{3+}$ = $La^{3+}$, $Sm^{3+}$, $Eu^{3+}$, $Gd^{3+}$, $Tm^{3+}$, $Yb^{3+}$) complexes with two fluorinated achiral tris(β-diketonate) ligands (HFA = hexafluoroacetylacetonate, TTA = 2-thenoyltrifluoroacetonate), and incorporating a chiral bis(oxazolinyl)pyridine (*PyBox*) unit as a neutral ancillary ligand, by the combined use of optical and chiroptical methods, ranging from UV to IR both in absorption and circular dichroism (CD) and including circularly polarized luminescence (CPL). Ultimately, all the spectroscopic information integrate into a total and a chiroptical super-spectrum, which allows one to characterize a multidimensional chemical space, spanned by the different $Ln^{3+}$ ion, the acidity and steric demand of the diketone and the chirality of the *PyBox* ligand. In all cases, $Ln^{3+}$ ions endow the systems with peculiar chiroptical properties, either allied to *f-f* transitions or induced by the metal onto the ligand. More in detail, we found that $Sm^{3+}$ complexes display interesting CPL features, which partly superimpose and partly integrate the more common $Eu^{3+}$ properties. Especially in the context of security tags, the pair Sm/Eu may be a winning choice for chiroptical barcoding.

## Introduction

Chiral trivalent lanthanide ($Ln^{3+}$) complexes find primary applications in extremely diverse areas of chemistry and material sciences: enantioselective catalysis,[1] biomedical imaging,[2] chiroptical analysis,[2c, 3] magnetism,[4] and luminescence.[5] At the basis of such a broad interest, there are some unique chemical and spectroscopic features of these elements, like for example variable coordination number and geometries, paramagnetism, extremely narrow absorption and emission lines with magnetic dipole and electric quadrupole character.[6] For long time, we have been interested in $Ln^{3+}$ chiroptical properties, in relation to the geometry of the complexes,[7] and recently, we further focused on circularly polarized luminescence (CPL).[8] Among many other applications, we may recall that $Ln^{3+}$-based CPL has been profitably used in the construction of circularly polarized OLEDs,[8b, 9] for bioanalytical assays and imaging[2a-d, 2f, 2g] and it has a great perspective in the development of security tags and anti-counterfeiting methods.[5g, 10] In order to take most advantage of CPL, beside high photoluminescence anisotropy factor ($g_{lum}$), the emitter must have a high extinction coefficient and quantum yield,[11] $g_{lum}$ is defined as

$$g_{lum} = 2 \cdot \frac{I_L - I_R}{I_L + I_R}$$

and measures the relative degree of polarization of the emitted photons ($I_L$ and $I_R$ are the intensities of left and right-circularly polarized light). A common illumination source to elicit luminescence is the 365 nm line of Hg lamps, which is also produced by inexpensive UV-B LEDs and ensures safe operation with minimal eye and skin protection. In this context, diketonates partly fulfil the high $B_{CP}$ requirement, because they usually display fairly good absorption at 365 nm and have suited triplet state to sensitize $Eu^{3+}$ and $Sm^{3+}$ red emission,[5g, 12] or even $Yb^{3+}$ in the NIR,[13] while they are less suited for $Tb^{3+}$. Among a very large whole family, HFA (hexafluoroacetylacetonate) and TTA (2-thenoyltrifluoroacetonate), shown in Chart 1, stand out, because of their optimal $Eu^{3+}$ sensitization due also to the very few (or no) protons in the close vicinity to the $Ln^{3+}$, which has the further merit of preventing one of the most significant sources of luminescence quenching, allied to C-H (as well as O-H and N-H) vibrational phonons.[6a, 14]

Recently, several chiral complexes appeared in literature, where the $Ln(HFA)_3$ coordination sphere is completed by a chiral ancillary ligand;[15] here we will consider pyridine bisoxazolines *PyBox* (Chart 1), a family of tridentate ligands.[16] Actually, $Ln(TTA)_3$ and $Ln(HFA)_3$ complexes can be easily prepared and they are relatively stable species, with 2 or 3 further coordination sites available. *PyBox* are tridentate ligands, able to fill the $Ln^{3+}$ coordination sphere of $Ln(HFA)_3$ or $Ln(TTA)_3$ and to endow it with well-defined chirality. This gives us the opportunity to work on a highly flexible scaffold of

[a] Dipartimento di Chimica e Chimica Industriale, Università di Pisa, via Moruzzi 13, 56124 Pisa, Italy. E-mail: lorenzo.dibari@unipi.it
[b] Institute of Organic Chemistry, Polish Academy of Sciences, ul. Kasprzaka 44/52, 01-224 Warsaw, Poland.

† Electronic Supplementary Information (ESI) available. See DOI: 10.1039/x0xx00000x

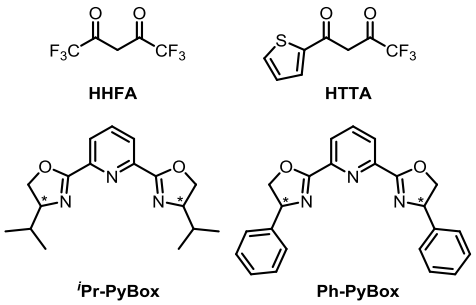


**Chart 1.** Structures of β-diketones (top) and *PyBox* ligands (bottom) employed for the screening of the chiroptical properties of $Ln^{3+}$ complexes.

formula Ln $L_3$ $L^*$, where the $Ln^{3+}$ can span the whole series, L represents a diketonate, and $L^*$ may be in principle *any PyBox*. This is interesting, because there are several chiral *PyBoxes* commercially available and a wider set can be obtained from inexpensive chirality pool compounds. In 2011, Yuasa et al. demonstrated that such strategy allows one to obtain luminescence complexes endowed with high quantum yield (41%) and high $g_{lum}$ (up to 0.46).[16a, 17]

In our study, we decide to investigate in-depth a set of $Ln^{3+}$ complexes ($Ln^{3+}$ = La, Sm, Eu, Gd, Tm, Yb) of two aforementioned β-diketonates, namely HFA and TTA (Chart 1), selected with respect to their different steric hindrance and acidity. As a chiral auxiliary ligand, two Bis(oxazoline)pyridines (*PyBox*), *e.g.* 2,6-Bis(4-isopropyl-2-oxazolin-2-yl) pyridine ($^i$PrPyBox) and 2,6-Bis(4-phenyl-2-oxazolin-2-yl) pyridine (PhPyBox) were used, since they are commercially available in both enantiomers.

Besides these properties, which can be considered metal-centred, a further aspect of interest relies in an induced property onto the organic ligand: which we dubbed lanthanide-induced vibrational CD (VCD) enhancement or LIVE.[18] We noticed that the VCD spectra of several paramagnetic $Ln^{3+}$ compounds display strong signals, which are nicely reproduced from one element to the other one. The theoretical basis to understand this effect is still missing, possibly also on account a somewhat limited number of experimental cases. To summarize, Fig. 1 schematically represents the utility of diverse chiroptical methods in a study of $Ln^{3+}$ complexes. Here absorption (ECD, VCD) and emission (CPL) chiroptical responses combine. In order to make this picture clearer and more practical, we emphasized the electromagnetic ranges in which each chiroptical method works, so that on *y*-axis we put the whole range from about 0.1 to 6 eV utilized by commercially available instruments, *i.e.* from the mid-IR (900 $cm^{-1}$) *via* the NIR and the VIS to the UV (200 nm). On *x*-axis, we indicate which of the 15 $Ln^{3+}$ ions, are amenable to each technique.

It is worth to stress that although CPL spectroscopy can be applied efficiently only for ~25% of overall of $Ln^{3+}$, *i.e.* $Eu^{3+}$, $Tb^{3+}$, $Sm^{3+}$, $Dy^{3+}$ and possibly[19] (but rarely) $Yb^{3+}$ and $Nd^{3+}$ in the commonly attainable measurement spectral range[8a] (VIS and a small part of NIR), this technique in comparison to CD is much more sensitive to the $Ln^{3+}$ environment and plays a critical role in the study of chiral $Ln^{3+}$.[20] Moreover, in the case of organic molecules usually absorption and emission dissymmetry factors are correlated[21] (if the electronic states involved in absorption and emission are not different), while in the case of $Ln^{3+}$, a prediction of the sign and magnitude of CPL cannot be inferred from their absorption properties alone, and therefore a more extended study of their chiroptical properties is required.

Since $Eu^{3+}$ complexes were largely investigated so far, in our examination we put primary importance on $Sm^{3+}$, $Tm^{3+}$ and $Yb^{3+}$. Additionally, to support some parts of discussion we obtained also analogous complexes with $La^{3+}$, $Eu^{3+}$ and $Gd^{3+}$.

We are well aware that CPL instruments are still not available in most laboratories and thus we were motivated to identify factors ensuring high $B_{CP}$, which is relevant for most practical applications and to provide easy and broadly amenable measurements that can guide the selection of good candidates to be submitted to CPL measurements.

## Results and Discussion

Interestingly, we could not find a satisfactory analysis of the ECD and VCD spectra of $^i$PrPyBox and PhPyBox, in spite of their widespread use in enantioselective synthesis.[1e, 22]

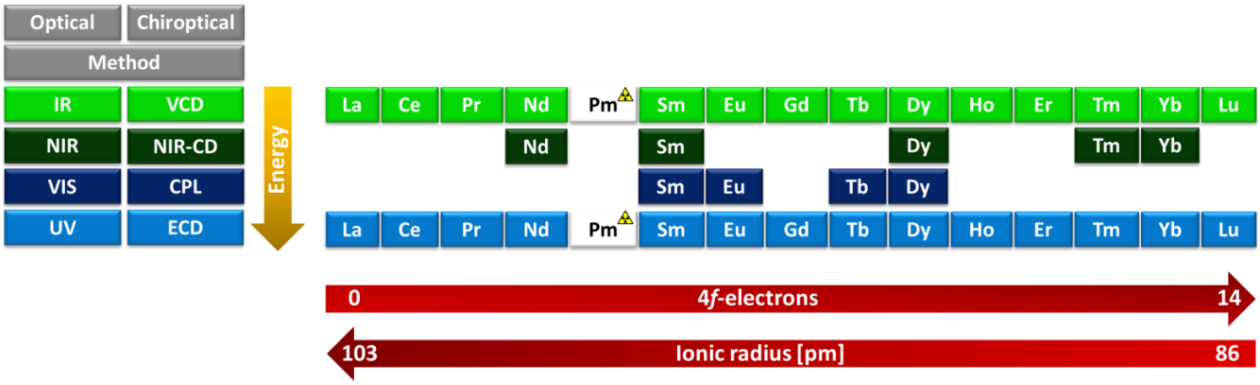


**Figure 1**. Representation of the utility of Ln3+ ions in the context of optical and chiroptical techniques. Notice that IR/VCD and UV/ECD refer to ligand-centred transitions and only NIR/NIR-CD or VIS/CPL refer to Ln3+-centered transition. To be precise, NIR-CD is a manifestation of electronic CD, because it is allied with *f-f* transitions. In common language, ECD normally refers to UV-VIS. The bottom arrows remind us the number of *f*-electrons of the $Ln^{3+}$ ion and the trend of the ionic radii.

For this reason, we provide experimental data of these chiral ligands and their interpretation in the ESI. They display similar ECD spectra: the main differences are in the intensity of bands, with PhPyBox giving ~2.5 times more intense bands with respect to $^{i}$PrPyBox. Also, the main sequence of VCD bands remains pretty similar. The most noticeable differences are in the narrow range 1500-1445 $cm^{-1}$, where the pyridine and -$CH_2$- vibrations from oxazolines are overlapped with C–H bending or C–C stretching vibrations due to $^{i}$Pr- or Ph- groups, respectively.

**Electronic CD**

UV and ECD spectra of Ln(TTA)$_3$-(*R*)-$^{i}$PrPyBox and Ln(TTA)$_3$-(*R*)-PhPyBox (Ln = La, Sm, Eu, Gd, Tm, Yb) in $CH_2Cl_2$ are presented in Fig. 2. The UV and ECD spectra of Ln(TTA)$_3$-(*R*)-$^{i}$PrPyBox and of Ln(TTA)$_3$-(*R*)-PhPyBox are consistent in terms of position of bands. As expected they are substantially different from those of the free *PyBox* ligand, as one can see, comparing Fig. 2 and Fig. S2 in ESI. The major absorption bands are dominanted by the π-π* transitions both from β-diketonate and the *PyBox* ligand. All $Ln^{3+}$, both with $^{i}$Pr- and Ph- ligand, show high coherence: the most prominent band is centered at ~345 nm, and two less intense ones are in the range of 250-300 nm, overlapped with the absorption band from free ligand. The noticeable intensity differences may be related to the presence of complex solvolysis, which is fast in very diluted solutions of $Ln^{3+}$ (spectra were recorded in ~0.4 mM), so the $Ln^{3+}$ complexes and the free β-diketone are simultaneously present in solution in variable ratio, mainly affecting the range 310-400 nm. As we shall see later, at much higher concentration (>10 mM, as used *e.g.* for NIR-CD or for VCD), solvolysis is not an issue, therefore all bands display almost identical magnitude.

For ECD (Fig. 2, left), the enantiomeric compounds give mirror-image profiles (ESI, Fig. S3). As expected, the intensity of ECD bands are fluctuating too, however, the main bands remain essentially the same as for position and relative amplitudes: two negative ones centered at ~295 nm and ~370 nm, and a positive one at ~275 nm. The order of magnitude of $|g_{abs}|$ factor for the band at ~335 nm is in the range of $4 - 8 \times 10^{-4}$. The homogeneity of these spectra upon changing the metal ion is consistent with other literature data and confirms that *f*-orbitals are not significantly mixed with the ligand ones. Only, the small variation of the size of $Ln^{3+}$ may slightly impact on the complex geometry and consequently be responsible for minor modulations of the ECD spectra. For the second set of complexes with the general formula Ln(HFA)$_3$-$^{i}$PrPyBox and Ln(HFA)$_3$-PhPyBox, as expected, the same structural homogeneity described for the TTA analogues is present (ESI, Fig. S4). The spectra are consistent with the ones reported by Yuasa et. al. for analogous $Eu^{3+}$ and $Tb^{3+}$ complexes.[16] Thus, for the sake of clarity and ease of comprehension in this section we shall keep the discussion mainly based on various $Sm^{3+}$ complexes, and the conclusions will be extended to analogous $Ln^{3+}$ complexes: all the experimental data on the other lanthanides we studied can be found in the Fig. S3 in ESI. In Fig. 3 we show the ECD and UV spectra of the two enantiomers of Sm $L_3$ $L^*$ in $CH_2Cl_2$ for both the complexes with L = HFA, TTA and $L^*$ = $^{i}$PrPyBox, PhPyBox ligands.

The UV spectra of Sm(HFA)$_3$-$^{i}$PrPyBox and Sm(HFA)$_3$-PhPyBox complexes are very similar and have one band centered at 308 nm, which is allied to HFA transitions. The same occurs for Sm(TTA)$_3$-$^{i}$PrPyBox and Sm(TTA)$_3$-PhPyBox, where the maximum UV is at ~345 nm, owing to the extended conjugation due to the thiophene group. Moreover, for the latter group a moderate increase of UV intensity is observed. With the exception of Sm(HFA)$_3$-$^{i}$PrPyBox,

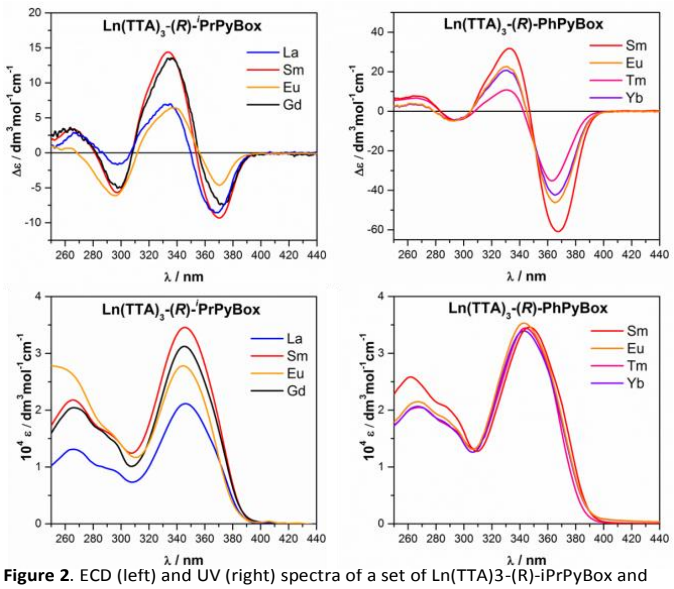


**Figure 2**. ECD (left) and UV (right) spectra of a set of Ln(TTA)3-(R)-iPrPyBox and Ln(TTA)3-(R)-Ph-PyBox (Ln = La, Sm, Eu, Gd, Tm, Yb) recorded in CH2Cl2.

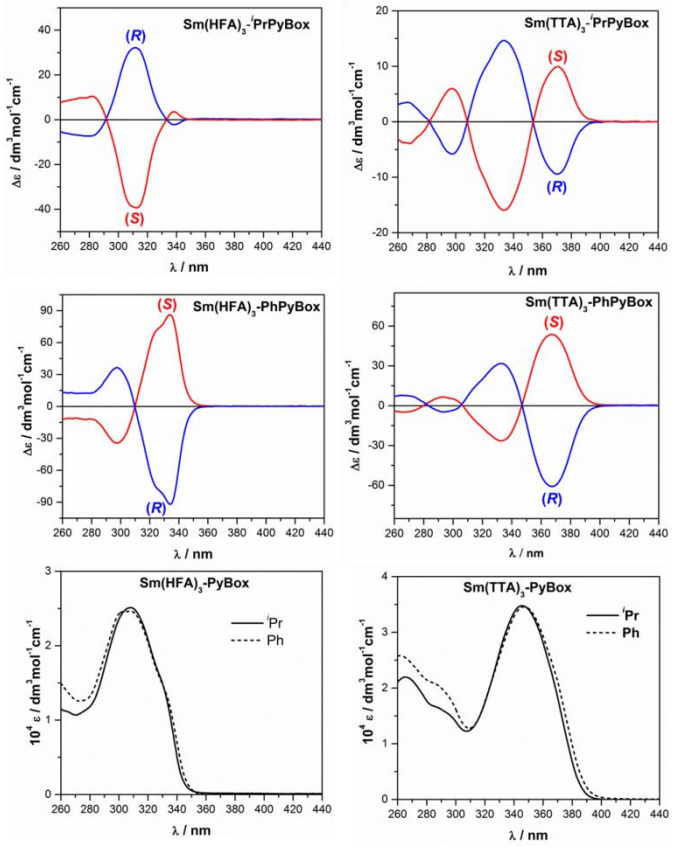


**Figure 3.** ECD and UV spectra of $Sm^{3+}$ complexes recorded in $CH_2Cl_2$.

the ECD spectra are characterized by a null point very close to the absorption maximum, which strongly calls for a degenerate exciton coupling between the $\pi-\pi^*$ transitions of the β-diketonate chromophore. So, the ECD spectra of Sm(TTA)$_3$-$^i$PrPyBox, Sm(TTA)$_3$-PhPybox and Sm(HFA)$_3$-PhPyBox show negative exciton couplets for the (*R*) enantiomers and positive ones for the (*S*) enantiomers. This is reasonably associated to the major electric transition dipole moment of β-diketonates, which is directed along the two oxygen atoms, and centered close to the central carbon of the diketonate. For Sm(HFA)$_3$-$^i$PrPyBox, the null point does not correspond to the UV maximum and the couplet feature cannot be assigned easily. At any rate, even if it has weak rotatory strength, the lowest energy transition (338 nm) is of the *same sign* as the corresponding couplets of all the analogous compounds. Indeed, we must recall that the complexes can belong at highest to a $C_2$ point group and thus the three diketonate ligands cannot be equivalent, thus possibly originating a situation which is more complex than a simple exciton couplet.

At least for $Yb^{3+}$ and $Tm^{3+}$, there are relevant electronic transitions in the NIR, where there are no contributions from ligand-centered contributions. Noteworthy, the ones around 975 nm for $Yb^{3+}$ ($^2F_{7/2}\rightarrow{}^2F_{5/2}$) and 1215 nm ($^3H_5\rightarrow{}^3H_6$) for $Tm^{3+}$ can be classified as *D I*, *i.e.* characterized by a strong dissymmetry factor, according to Richardson.[23] Fig. 4 displays the NIR-CD and associated absorption spectra. In all cases, only one line is clearly apparent, in spite of the fact that higher multiplicity of the terms may be expected.[6b]

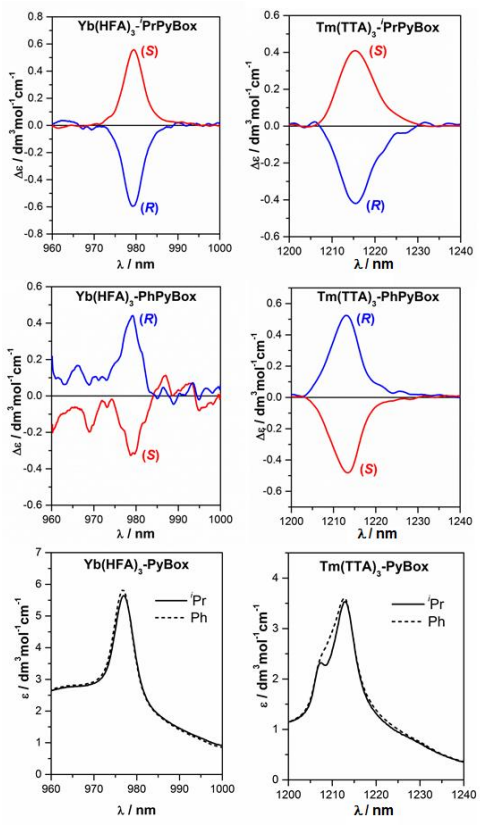


**Figure 4.** NIR-CD and NIR spectra of $Yb^{3+}$ (left) and $Tm^{3+}$ (right) complexes recorded in $CH_2Cl_2$.

We should underline that there are very only few NIR-CD spectra of $Tm^{3+}$ $^3H_6\rightarrow{}^3H_5$ transition previously reported in the literature.[8a] For all cases, we observe the remarkably high dissymmetry factor $g_{abs}$ ≈ 0.1.

**Circularly polarized luminescence**

Similarly to what we have seen by NIR-CD, CPL has the distinct feature of selectively responding only to the suitable chiral non-racemic $Ln^{3+}$ species, in contrast to ECD or VCD, which may respond to free as well as to bound ligands.[3b, 6b] In practice, among the $Ln^{3+}$ complexes under investigation, in the spectral range (VIS) available to our analysis only $Sm^{3+}$ and $Eu^{3+}$ are active. Naturally, we decided to further probe their 3D structure, and in the next step select system(s) with the highest $|g_{lum}|$ factors. As stated before, in our study we gave priority to $Sm^{3+}$, since in the literature only little attention has been paid to its CPL activity and only a few examples are reported.[12, 24] The largest $|g_{lum}|$ factor of $Sm^{3+}$ reported so far is for Cs[Sm((+)-hfbc)$_4$] and amounts to 1.15 at 553 nm.[12]

The most obvious starting point is to record CPL and PL spectra of both enantiomers within two target sets of complexes under investigation, *i.e.* Sm(HFA)$_3$-PyBox and Sm(TTA)$_3$-PyBox. In Fig. 5, we plotted separately the CPL and PL spectra measured in $CH_2Cl_2$ for both $^i$PrPyBox and PhPyBox ligands. The PL and CPL spectra in the range of 540-700 nm are characterized by the three well-separated

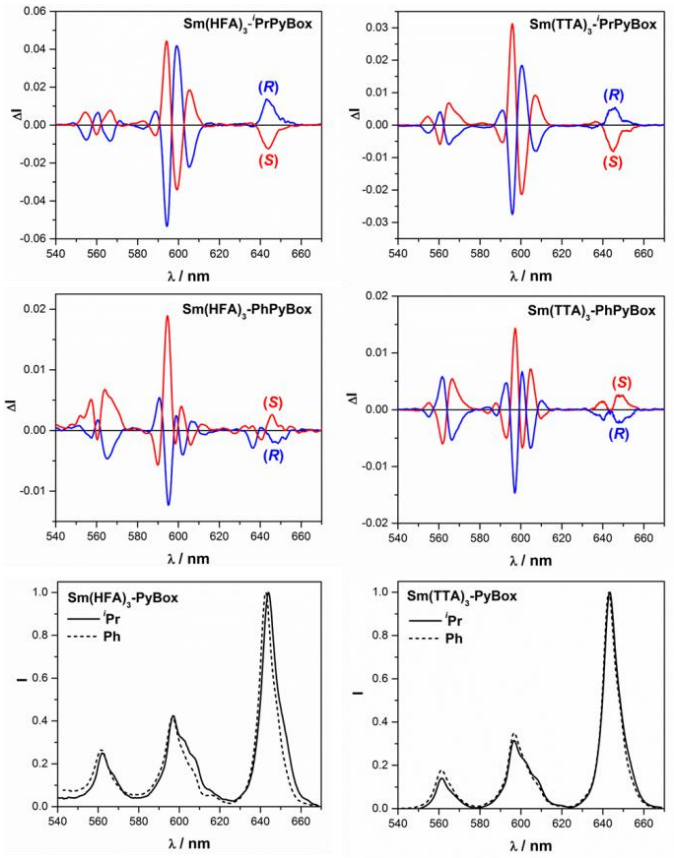


**Figure 5.** CPL and PL spectra of both enantiomers of Sm(HFA)$_3$-PyBox and Sm(TTA)$_3$-PyBox recorded in $CH_2Cl_2$. The spectra were normalized with respect to the $^4G_{5/2}\rightarrow{}^6H_{9/2}$ transition at 640 nm.

transitions, characterized by the three well-separated transitions, *i.e.* $^4G_{5/2}\rightarrow{}^6H_{5/2}$ at 561 nm (magnetic-dipole allowed), $^4G_{5/2}\rightarrow{}^6H_{7/2}$ at 596 nm (magnetic-dipole allowed), and $^4G_{5/2}\rightarrow{}^6H_{9/2}$ at 643 nm (magnetic-dipole forbidden). Within each spectroscopic term, CPL spectra display richer multiplets than PL counterparts, thanks to the increased resolution stemming from the changeable sign of chiroptical signals.[8a]

In order to quantify the obtained data, in Tab. 1 we summarized the $|g_{lum}|$ factors for all the CPL bands recorded. The highest $|g_{lum}|$ factors for $Sm^{3+}$ at the most intense CPL transition at 595 nm are observed for complexes with $^i$PrPyBox, *i.e.* $Sm(HFA)_3$-(*R*)-$^i$PrPyBox and $Sm(TTA)_3$-(*R*)-$^i$PrPyBox, and amount to |0.18| and |0.10|, respectively. In contrast, for complexes with PhPyBox, *i.e.* $Sm(HFA)_3$-(*R*)-PhPyBox and $Sm(TTA)_3$-(*R*)-PhPyBox, this value is smaller (~0.035). This difference may tentatively be assigned to a somewhat bigger structural manifold for the PhPyBox than for $^i$PrPyBox complexes.[6b] This may be associated with the different number of conformers displayed by the free ligands, whereby $^i$PrPyBox is well represented by a single species, PhPyBox is spread into three conformers, as seen in ESI on Fig. S1.

In Fig. 6 displays the CPL and PL spectra for $Eu(TTA)_3$-(*R*)-$^i$PrPyBox and $Eu(TTA)_3$-(*R*)-PhPyBox recorded in $CH_2Cl_2$ (the HFA analogues were reported previously by Yuasa[16a]).

In contrast to $Sm^{3+}$ complexes, almost full mirrored-relationship of CPL signals are observed between $Eu^{3+}$ complexes with (*R*)-absolute configuration of *PyBox* ligands. The highest $|g_{lum}|$ value is measured at 595 nm and amounts to |0.24| for $Eu(TTA)_3$-$^i$PrPyBox, which is comparable with previously published one for $Eu(HFA)_3$-$^i$PrPyBox ($|g_{lum}|$ = |0.46|).[16a] The relative values of $|g_{lum}|$ factors for $^i$PrPyBox *vs.* PhPyBox for $Eu^{3+}$ complexes follow the same trend observed with $Sm^{3+}$.

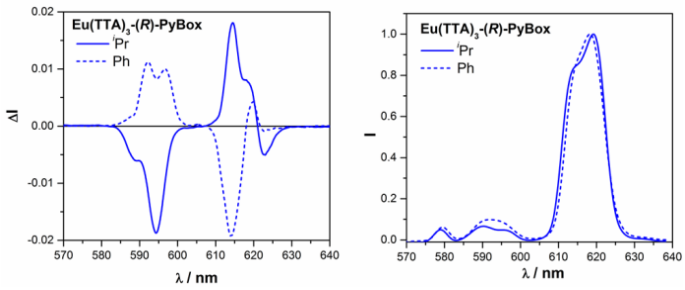


**Figure 6.** Normalized CPL (top) and PL (bottom) spectra of $Eu(TTA)_3$-(*R*)-$^i$Pr-PyBox and $Eu(TTA)_3$-(*R*)-Ph-PyBox recorded in $CH_2Cl_2$. The spectra were normalized with respect to the $^5D_0\rightarrow{}^7F_2$ transition at 614 nm.

## Vibrational CD

It is well known that VCD spectra display weak bands, which are usually from $10^{-5}$ to $10^{-4}$ times smaller than the relative IR absorptions. As early as in 1980, Mason reported that some complexes of *d*-block elements, *i.e.* $Ni^{2+}$ and $Co^{2+}$, display enhanced VCD signals.[25] There is now a substantial body of research on this topic, which has been discussed and examined extensively using plenty of examples.[26] Nevertheless, the origin of this phenomena is still not entirely clear. In 2012, we reported that some lanthanide chelates display conserved sequences of enhanced VCD bands throughout the $Ln^{3+}$ series (Lanthanide Induced VCD Enhancement, LIVE) and as a function of the electronic configuration of $Ln^{3+}$.[18] We observed that the spectra of $Yb^{3+}$ and $Tm^{3+}$ complexes are strongly enhanced compared with those of $La^{3+}$ ($4f^0$), $Gd^{3+}$ ($4f^7$) and $Lu^{3+}$ ($4f^{14}$), which on the contrary display usual intensities of the bands.

The foremost scope of this section is to check whether we can disclose more details about the LIVE phenomena on our set of chiral complexes.

Experimental VCD and IR spectra collected in the range between 2000 and 950 $cm^{-1}$ in $CDCl_3$ using the set of enantiomeric Ln-complexes together with spectra of chiral *PyBox* ligands are provided in Fig. 7.

All complexes under investigation exhibit much stronger VCD and IR intensities with respect to the *PyBox* ligands, so for an easier comparison on Fig. 7 we multiplied these data by 25 and 5, respectively. IR spectra of $Ln^{3+}$ complexes with HFA and TTA in terms of ε values reach 3700 and 2200 $dm^3mol^{-1}cm^{-1}$, respectively. On the contrary, $\varepsilon_{max}$ intensity of *PyBox* ligands is limited to ~400 $dm^3mol^{-1}cm^{-1}$. IR spectra of $Ln^{3+}$ complexes ($Sm^{3+}$, $Tm^{3+}$, $Yb^{3+}$) are very different from *PyBox* ligands. However, one may find some similarities by comparing spectra within the two sub-families of $Ln^{3+}$ (HFA *vs.* TTA) to those of *PyBox* ligands.

**Table 1.** Summary of CPL data by using dissymmetry factors $|g_{lum}|$ derived from spectra of $Sm^{3+}$ and $Eu^{3+}$ of two investigated families of $Ln(TTA)_3$-(*R*)-PyBox and $Ln(HFA)_3$-(*R*)-PyBox (Ln = Sm, Eu) recorded in $CH_2Cl_2$. Note: # taken from Ref. [16a].

| Complex | $\|g_{lum}\|$ factor | | | | |
|---|---|---|---|---|---|
| | $^4G_{5/2}\rightarrow{}^6H_{5/2}$ ~560 nm | $^4G_{5/2}\rightarrow{}^6H_{7/2}$ ~595 nm | $^4G_{5/2}\rightarrow{}^6H_{9/2}$ ~645 nm | $^5D_0\rightarrow{}^7F_1$ ~595 nm | $^5D_0\rightarrow{}^7F_2$ ~614 nm |
| $Sm(HFA)_3$(*R*)-$^i$Pr-PyBox | 0.05 | 0.18 | 0.013 | | |
| $Sm(HFA)_3$(*R*)-Ph-PyBox | 0.03 | 0.03 | 0.003 | | |
| $Sm(TTA)_3$(*R*)-$^i$Pr-PyBox | 0.08 | 0.10 | 0.008 | | |
| $Sm(TTA)_3$(*R*)-Ph-PyBox | 0.03 | 0.04 | 0.002 | | |
| $Eu(HFA)_3$(*R*)-$^i$Pr-PyBox# | | | | 0.46 | 0.03 |
| $Eu(HFA)_3$(*R*)-Ph-PyBox# | | | | 0.15 | 0.02 |
| $Eu(TTA)_3$(*R*)-$^i$Pr-PyBox | | | | 0.24 | 0.02 |
| $Eu(TTA)_3$(*R*)-Ph-PyBox | | | | 0.11 | 0.01 |

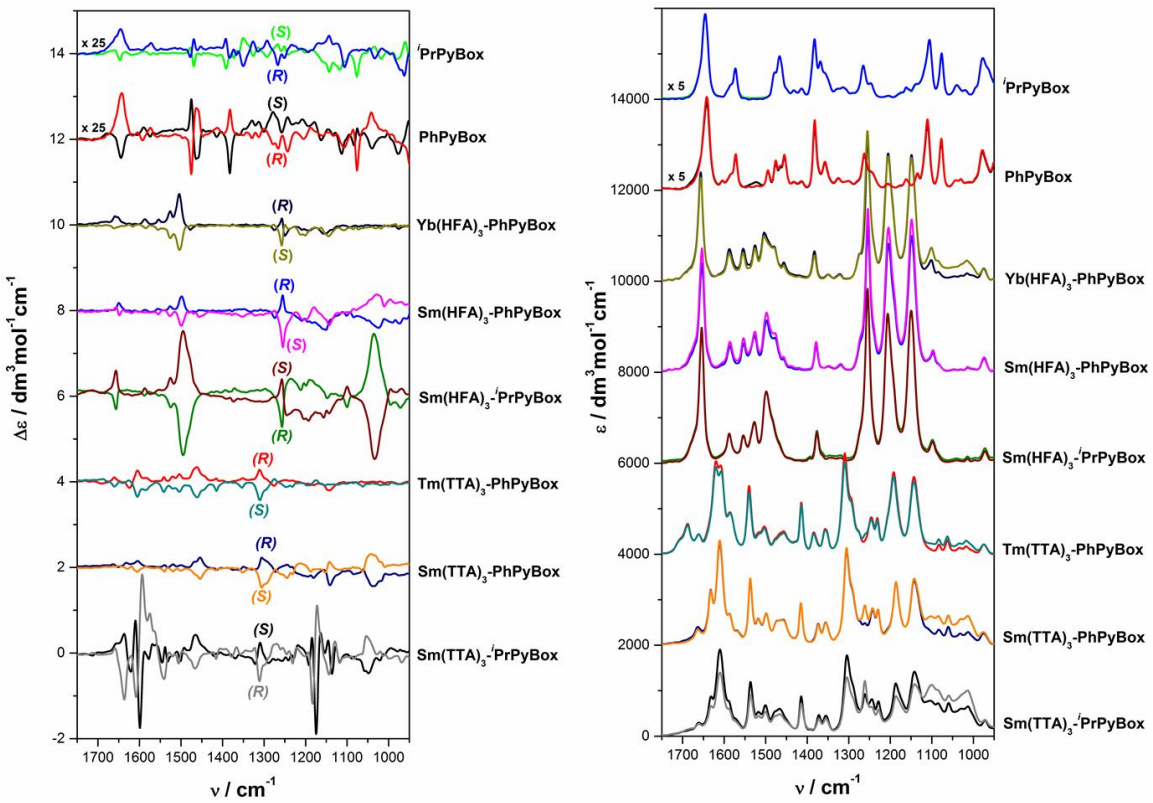


**Figure 7.** VCD (left) and IR (right) spectra of enantiomers of $Ln^{3+}$ complexes recorded in $CDCl_3$ compared to enantiomers of $^{i}$PrPyBox and PhPyBox ligands.

VCD spectra of enantiomers are mirror image and show strong correspondences to the relevant IR. VCD spectra of $Ln^{3+}$ complexes in terms of $\Delta\varepsilon$ values are much stronger than usual: for most bands $|\Delta\varepsilon|$ are ranging from 0.3 to 0.7 $dm^3mol^{-1}cm^{-1}$, with the maximum ~1.5 $dm^3mol^{-1}cm^{-1}$ observed only for $Sm(HFA)_3$-$^{i}$PrPyBox. This clearly indicates the enhancement of VCD signal. The $|g_{abs}|$ values amount to an average of $\sim10^{-4}$ for the most prominent bands, which is about 10-times higher than the free ligands. A more detailed examination revealed that the $g_{abs}$ fluctuates and depends on the complex. The highest values are observed for $Sm^{3+}$ at ~1035 $cm^{-1}$, *i.e.* $Sm(HFA)_3$-$^{i}$PrPyBox ($|g_{abs}|=1.5\times10^{-2}$), $Sm(HFA)_3$-PhPyBox ($|g_{abs}|=6.0\times10^{-3}$) and $Sm(TTA)_3$-PhPyBox ($|g_{abs}|=2.0\times10^{-3}$). As a consequence, we were able to collect all the VCD spectra, with a very high S/N ratio, within only 10 minutes, which in comparison to typical VCD measurement (up to a few hours) for organic compounds is an extremely short acquisition time.

As shown in Fig. 7, complexes with HFA give main VCD bands centered at ~1655, ~1500, ~1256 and ~1035 $cm^{-1}$ (the latter one is silent for $Yb(HFA)_3$-PhPyBox) which are attributed to the oxazoline rings and β-diketonate moiety. In the second family of complexes with TTA, the most characteristic bands are at ~1605, ~1462, ~1310 $cm^{-1}$, and for $Sm(TTA)_3$-(*R*)-PhPyBox and $Sm(TTA)_3$-(*R*)-$^{i}$PrPyBox also ~1140 and ~1040 $cm^{-1}$. This indicates clearly structural uniformity within both families, and shows that all complexes have a well-defined conformation, which is indeed frozen in a clear pattern of VCD spectrum, *ipso facto* confirming that the replacement of $Ln^{3+}$ ions does not affect the vibrational structure of our systems. The VCD features resemble each other in the region of 1315-1255 $cm^{-1}$, corresponding with the two oxazoline rings vibrations, therefore we shall analyze their 3D structure using only this region. In VCD spectra with TTA there is one band in the range 1315-1308 $cm^{-1}$ which is positive for $Sm(TTA)_3$-(*S*)-$^{i}$PrPyBox, and negative for both $Sm(TTA)_3$-(*S*)-PhPyBox and $Tm(TTA)_3$-(*S*)-PhPyBox. The same observation can be derived from the series of $Ln^{3+}$ with HFA, in the slightly different range, *i.e.* 1258-1255 $cm^{-1}$. Analogously, the VCD spectrum of $Sm(HFA)_3$-(*S*)-$^{i}$PrPyBox gives a positive Cotton Effect (CE), while complexes containing (*S*)-PhPyBox, *i.e.* $Yb(HFA)_3$-(*S*)-PhPyBox and $Sm(HFA)_3$-(*S*)-PhPyBox, present a negative one.

To recap: the VCD results indicate pronounced evidence on conformational homogeneity within the investigated series, further confirming conclusions derived from the ECD spectra.

Calculations of vibrational properties are based on the ground-state electronic structure, and they are considered to be more reliable and easily captured by DFT simulations than their electronic properties, which require accurate prediction of excited-state transitions. This is particularly true for metal complexes. In order to gain more insight into the relationship between the IR/VCD features and structural properties of Ln-complexes in solution, we used as input geometries the X-ray structures previously published by Yuasa of $Tb(HFA)_3$-(*S*)-$^{i}$PrPyBox and $Tb(HFA)_3$-(*S*)-PhPyBox.[16a] In the first step we built our model by exchanging Tb with La, which is included into commonly used functional and basis set used in DFT simulations of vibrational transitions. Next, we submitted the obtained model structures to geometry optimization, followed by IR/VCD calculations. The calculations were carried out using the B3LYP functional, and 'mixed' basis sets: 6-31G(d) for H, C, N, O, F

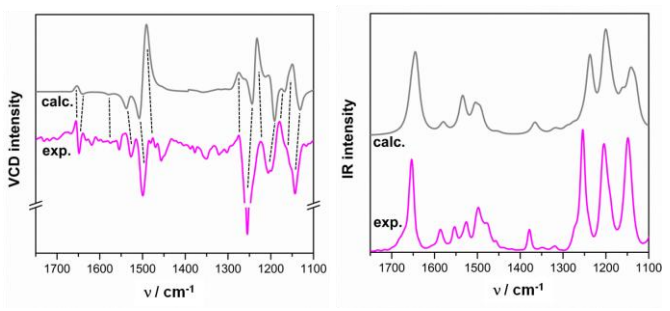


**Figure 8.** DFT calculated VCD (left) and IR (right) spectra for La(HFA)$_3$-(*S*)-PhPyBox compare to experimental spectra of Sm(HFA)$_3$-(*S*)-PhPyBox; Calculations run at the B3LYP functional, and 6-31G(d) basis set for H, C, N, O, F and the LanL2DZ for La; frequencies scaled by a factor 0.965; Lorentzian band-width $\sigma$ = 10 cm$^{-1}$. The spectra are shown with a vertical offset for better clarity; the range of 1400-1100 cm$^{-1}$ was multiplied by 2.

and LanL2DZ for La. Fig. 8 shows the comparison between the experimental (for $Sm^{3+}$) and calculated (for $La^{3+}$) VCD and IR spectra of Ln(HFA)$_3$-(*S*)-PhPyBox. In ESI, one can find results for the second model used, *i.e.* La(HFA)$_3$-(*S*)-$^{i}$PrPyBox.

The agreement between calculated and experimental IR/VCD spectra is acceptable, making allowances for at least two facts: (i) theoretical models for DFT calculations do not take into account the effect of LLES; (ii) we used two ('mixed') basis sets. Despite these limitations it is clear that both our model and level of calculations are truthful enough to make a reliable assignment of all bands. In the calculated VCD spectrum, however, there are some inconsistencies mainly in the range of 1485-1465 cm$^{-1}$ and 1200-1150 cm$^{-1}$. They are possibly related to the cancellation of vibrational transitions due to overlap of oppositely signed bands from the achiral HFA ligand. Calculations for Sm(HFA)$_3$-(*S*)-PhPyBox and Sm(HFA)$_3$-(*S*)-$^{i}$PrPyBox complexes using the SDD pseudopotential (ESI, Fig. S5), although very time-consuming, do not reproduce satisfactory all VCD bands, and DFT calculations are ultimately confirmed superior. For a more detailed examination of the relevant intensities of VCD bands, in Fig. 9A we extended the comparison to $Gd^{3+}$ and $La^{3+}$, where no VCD enhancement had been reported before.[18]

When we take into account these two ions, it appears clear that we can separate three different regions: one around 1600 cm$^{-1}$, one around 1200 cm$^{-1}$ and a broad one between them. While the former two display strong signals for the whole set of spectra, albeit with a remarkably modest activity for $La^{3+}$, the region in the middle is by far dominated by $Yb^{3+}$ and $Tm^{3+}$, with intensities about one order of magnitude larger than $La^{3+}$ and $Gd^{3+}$ (remember that the IR spectra are practically identical). Here again, we may observe that the $La^{3+}$ complexes display the weakest VCD intensities, which are generally not more than half of the ones of the other ions. On the other hand, $Gd^{3+}$ is somehow weaker in the 1600 cm$^{-1}$ region but of a similar magnitude as $Sm^{3+}$, $Yb^{3+}$ or $Tm^{3+}$ in proximity to 1200 cm$^{-1}$ which again confirms the LIVE effect, we described in ref. [18].

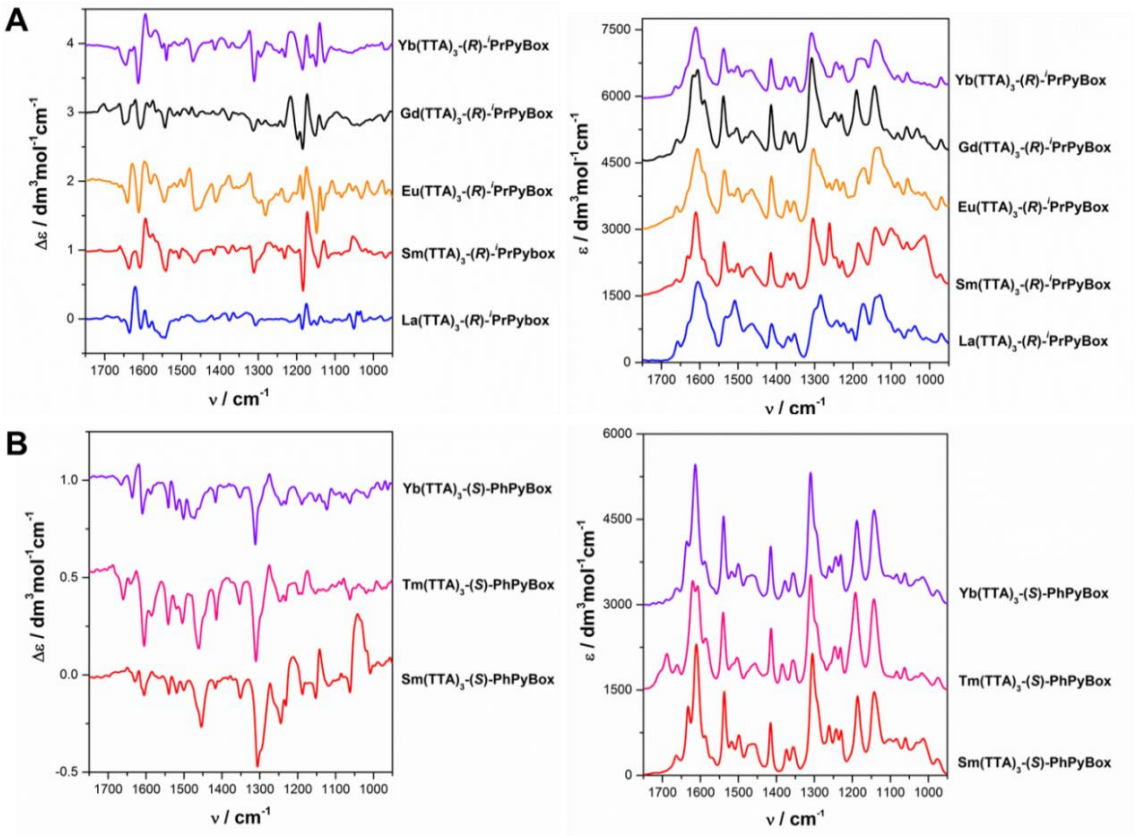


**Figure 9.** VCD (left) and IR (right) spectra of (**A**) Ln(TTA)$_3$-(*R*)-$^{i}$PrPyBox and (**B**) Ln(TTA)$_3$-(*S*)-PhPyBox (Ln = La, Sm, Eu, Gd, Tm, Yb) recorded in $CDCl_3$.

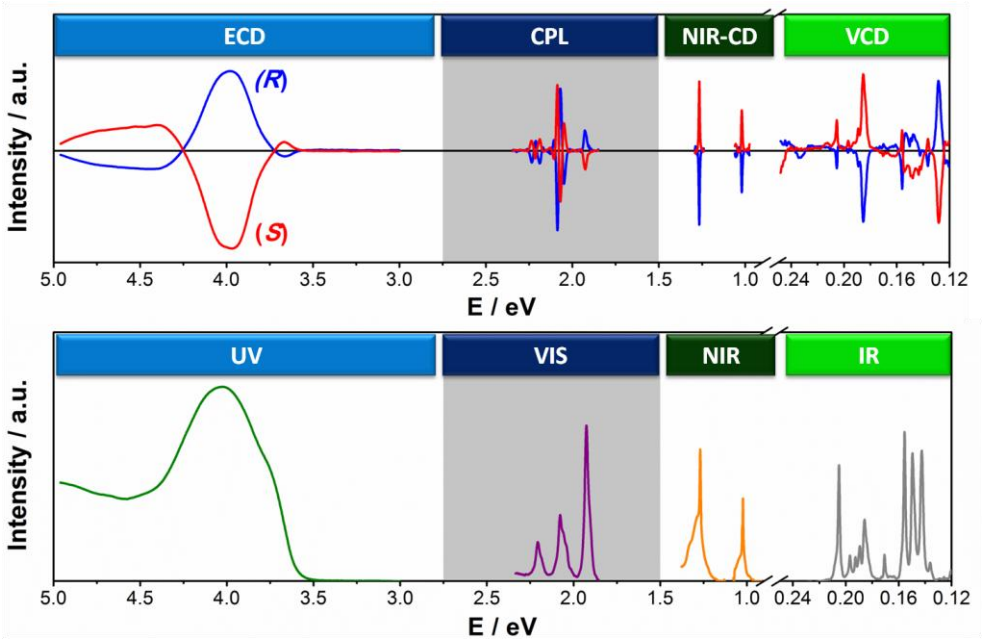


**Figure 10.** The idea of super-lanthanide probed by chiroptical (top) and optical (bottom) super-spectrum. See Experimental Section for measurements conditions.

**The super-spectrum of the super-lanthanide**

We collected and discussed a manifold of chiroptical data of a whole set of structurally homogeneous complexes. In the case of UV-ECD, where the transitions are genuinely ligand-centered, all complexes display comparable features and practically one may change lanthanide without even noticing. In the IR, the situation is slightly more complex, owing to the VCD enhancement, which is brought about by some ions more than by other ones, notably conserving the overall shape (at least region-by-region). Here again, the vibrational transitions are to be considered ligand-centered, but they experience an enhancement, thanks to the coupling with metal centered properties. In other spectral fields, namely in the VIS and in the NIR, the transitions are fully metal-centered and thus each and every lanthanide may or may not contribute with a completely distinct spectrum.

Recently, the concept of chiroptical super-spectrum has been introduced,[27] by making a cut-and-paste of spectra measured on different instruments in different fields *on the same compound.* Here, we wish to reproduce this concept introducing one more degree of freedom, by treating a structurally homogeneous set of $Ln^{3+}$ complexes as a single one, *i.e.* surfing between different ions in each spectral region. This is ultimately presented in Fig. 10, which is a pastiche of data taken on several complexes but is the most complete chiroptical fingerprint of our complexes and entangles the stereochemical information into one figure.

## Conclusions

We addressed the problem of finding lanthanides with relevant CPL, which means at the same time high brilliance and high light polarization. A good strategy appears to use ternary species, with an extremely efficient achiral sensitizer for a given lanthanide and a chiral multidentate ligand, which provides the necessary dissymmetry to the system. Presently we focused on red-emitting compounds, where we found that $Eu^{3+}$ and $Sm^{3+}$ homologue compounds both display strong and distinct CPL lines, in the same spectral region, which lends itself to information transfer, including cryptography and barcoding.

Thanks to a set of chiroptical spectra (ECD, NIR-CD, VCD), we observed, that these complexes have homogenous structures, which is clearly evidenced in (very) similar patterns of chiroptical spectra. We wish to underpin that we included in our analysis $Sm^{3+}$ CPL and $Tm^{3+}$ NIR-CD, which have been only rarely reported to-date, although they display interesting features and deserve not to be neglected in the future for their promising further practical applications.

Our investigation disclosed that $Ln^{3+}$ complexes are very easily handled by VCD spectroscopy. Even though additional investigations are needed to learn more about the LIVE phenomenon, our findings show beyond question that this effect is highly suited to gain insight into the solution structures of newly designed $Ln^{3+}$ complexes. This may be interesting in a fast screening study for seeking eligible properties, which in literature is still a very rare strategy.

This study provides a platform for the development of 3D structure-spectral correlations in solution, linking lanthanide emission and absorption chiroptical spectroscopies. This easy-to-handle route will enable one to characterize $Ln^{3+}$ and can be invaluable when the X-ray structure in not available.

## EXPERIMENTAL SECTION

**General**

All reagents were purchased from commercial sources (Sigma Aldrich, Alfa Aesar) at highest available purity and used without

further purification. The structures of the obtained compounds were confirmed by optical and chiroptical spectroscopies.

**Spectroscopy**

ECD and UV spectra were measured using a Jasco J–710 spectropolarimeter in the range of 190-800 nm in spectroscopic grade solvents in various quartz cells. All spectra were registered using a scanning speed of 100 nm $min^{-1}$, a step size of 0.2 nm, a bandwidth of 2 nm, a response time of 1 s, and 4 scans. The spectra were background–corrected using solvent spectra recorded under the same conditions.

NIR-CD spectra were measured using a Jasco J-200D spectropolarimeter in the range of 800-1300 nm in spectroscopic grade $CH_2Cl_2$ (~16 mM) in a quartz cell with a path length of 1 cm. All spectra were registered using a scanning speed of 50 nm $min^{-1}$, a step size of 0.2 nm, a bandwidth of ca. 10 nm, a response time of 2 s, and an accumulation of 3 scans. The spectra were background–corrected using spectra of solvent recorded under the same conditions.

NIR spectra were recorded in the range of 800-1300 nm in spectroscopic grade $CH_2Cl_2$ (~16 mM) in a quartz cell with a path length 1 cm. All spectra were measured using a scanning speed of 100 nm $min^{-1}$, a step size of 0.2 nm, a bandwidth of 8 nm, a fast response time, and an accumulation of 3 scans. The spectra were background–corrected using spectra of solvent recorded under the same conditions.

CPL and PL measurements were recorded using our home-built CPL spectrofluoropolarimeter described in Ref.[28] All solutions in $CH_2Cl_2$ with concentration ~10 mM were placed in 1 cm cell, and irradiated by a fluorescent UV lamp ($\lambda_{exc}$ = 365 nm) using 90° geometry. CPL and PL spectra were recorded using a scanning speed of 20 nm/min, an emission slit width of ~4 nm, an integration time of 2 s; each spectrum is the average of 3 accumulations. All CPL spectra were normalized to the corresponding PL intensity band in the emission spectrum, which was recorded together with CPL. The dissymmetry factor $g_{lum}$ was determined according to the definition given in the Introduction.

VCD and IR spectra were recorded in $CDCl_3$ solution placed in $BaF_2$ cell (100 μm) using a Jasco FVS–6000 (Tokyo, Japan) spectrometer with 4 $cm^{-1}$ resolution in the range of 2000–850 $cm^{-1}$. The PEM was set at 1400 $cm^{-1}$ for all measurements. The spectra were carried out within 10 min (1000 scans) in the case of $Ln^{3+}$ complexes using concentration ~40 mM, and for 2 h (12000 scans) for *PyBox* ligands with solution concentration ~0.17 M. The spectra were background–corrected using spectra of $CDCl_3$ recorded under the same conditions. The VCD/IR spectra were background-corrected by subtraction of the solvent spectrum measured under the same conditions.

**Computational details**

As an input geometry X-ray structures of $Tb(HFA)_3$-(*S*)-$^{i}$PrPyBox and $Tb(HFA)_3$-(*S*)-PhPyBox[16a] published by Yuasa were modified by replacing Tb for La. Then, they were submitted for DFT optimizations in Gaussian'09 (Revision D.01. Gaussian, Inc: Wallingford, CT; 2013), with default grids and convergence criteria, using B3LYP functional, and two basis sets: 6-31G(d) for H, C, N, O, F and LanL2DZ for La. In the next step, at the same level of theory VCD and IR spectrum was calculated and visualized using Lorentzian functions with a half-width at half height of 6 $cm^{-1}$, and a frequency scale factor of 0.965. Furthermore, DFT calculations were repeated based on aforementioned X-ray structure by using another model in which Tb was exchanged for Sm. Calculations were run using B3LYP functional, 6-31G(d) basis sets for H, C, N, O, F and the MWB28 pseudopotentials for Sm. The results are similar to those obtained using LanL2DZ basis set for La, so for the sake of clarity we take into considerations only these data.

## Conflicts of interest

There are no conflicts to declare.

## Acknowledgements

M.G. gives thanks for the support from the Polish Ministry of Science and Higher Education ('Mobilnosc Plus' grant no. 1286/MOB/IV/2015/0). All computational calculations were carried out at Wroclaw Centre for Networking and Supercomputing (WCSS) in Poland.

## References

1. (a) J. Inanaga, H. Furuno and T. Hayano, *Chem. Rev.*, 2002, **102**, 2211-2226; (b) H. C. Aspinall, *Chem. Rev.*, 2002, **102**, 1807-1850; (c) F. T. Edelmann, *Chem. Soc. Rev.*, 2012, **41**, 7657-7672; (d) M. Hatanaka and K. Morokuma, *ACS Catal.*, 2015, **5**, 3731-3739; (e) H. C. Aspinall, in *Chiral Lewis Acids in Organic Synthesis*, ed. J. Mlynarski, Wiley, 2017, pp. 261-298.
2. (a) M. C. Heffern, L. M. Matosziuk and T. J. Meade, *Chem. Rev.*, 2014, **114**, 4496-4539; (b) S. V. Eliseeva and J.-C. G. Bünzli, *Chem. Soc. Rev.*, 2010, **39**, 189-227; (c) J. Yuasa, T. Ohno, H. Tsumatori, R. Shiba, H. Kamikubo, M. Kataoka, Y. Hasegawa and T. Kawai, *Chem. Commun.*, 2013, **49**, 4604-4606; (d) J.-C. G. Bünzli, *J. Lumin.*, 2016, **170**, 866-878; (e) J. He, C. S. Bonnet, S. V. Eliseeva, S. Lacerda, T. Chauvin, P. Retailleau, F. Szeremeta, B. Badet, S. Petoud, E. Tóth and P. Durand, *J. Am. Chem. Soc.*, 2016, **138**, 2913-2916; (f) S. Shuvaev, M. Starck and D. Parker, *Chem. Eur. J.*, 2017, **23**, 9974-9989; (g) I. Martinić, S. V. Eliseeva and S. Petoud, *J. Lumin.*, 2017, **189**, 19-43; (h) I. Martinic, S. V. Eliseeva, T. N. Nguyen, F. Foucher, D. Gosset, F. Westall, V. L. Pecoraro and S. Petoud, *Chem. Sci.*, 2017, **8**, 6042-6050.
3. (a) S. Yamamoto and P. Bouř, *Angew. Chem. Int. Ed.*, 2012, **51**, 11058-11061; (b) R. Carr, N. H. Evans and D. Parker, *Chem. Soc. Rev.*, 2012, **41**, 7673-7686; (c) T. Wu, J. Kapitán, V. Mašek and P. Bouř, *Angew. Chem. Int. Ed.*, 2015, **54**, 14933-14936; (d) O. Kotova, S. Blasco, B. Twamley, J. O'Brien, R. D. Peacock, J. A. Kitchen, M. Martinez-Calvo and T. Gunnlaugsson, *Chem. Sci.*, 2015, **6**, 457-471; (e) T. Wu, J. Průša, J. Kessler, M. Dračínský, J. Valenta and P. Bouř, *Anal. Chem.*, 2016, **88**, 8878-8885; (f) D. Parker, S. Shuvaev, K. Mason and E. Suturina, *Chem. Sci.*, 2018, DOI: 10.1039/c1038sc00482j; (g) M. Leonzio, A. Melchior, G. Faura, M. Tolazzi, M. Bettinelli, F. Zinna, L. Arrico, L. Di Bari

and F. Piccinelli, *New J. Chem.*, 2018, DOI: 10.1039/C1037NJ04640E.

4. (a) R. Sessoli and A. K. Powell, *Coord. Chem. Rev.*, 2009, **253**, 2328-2341; (b) D. N. Woodruff, R. E. P. Winpenny and R. A. Layfield, *Chem. Rev.*, 2013, **113**, 5110-5148; (c) C.-H. Chen, D. S. Krylov, S. Avdoshenko, F. Liu, L. Spree, R. Yadav, A. Alvertis, L. Hozoi, K. Nenkov, A. Kostanyan, T. Greber, A. U. B. Wolter and A. A. Popov, *Chem. Sci.*, 2017, **8**, 6451-6465; (d) P. Zhang, M. Perfetti, M. Kern, P. P. Hallmen, L. Ungur, S. Lenz, M. R. Ringenberg, W. Frey, H. Stoll, G. Rauhut and J. van Slageren, *Chem. Sci.*, 2018, **9**, 1221-1230; (e) S. G. Miralles, A. Bedoya-Pinto, J. J. Baldovi, W. Canon-Mancisidor, Y. Prado, H. Prima-Garcia, A. Gaita-Arino, G. Minguez Espallargas, L. E. Hueso and E. Coronado, *Chem. Sci.*, 2018, **9**, 199-208.
5. (a) J. L. Lunkley, D. Shirotani, K. Yamanari, S. Kaizaki and G. Muller, *J. Am. Chem. Soc.*, 2008, **130**, 13814-13815; (b) G. Muller, *Dalton Trans.*, 2009, 9692-9707; (c) J.-C. G. Bünzli, *Coord. Chem. Rev.*, 2015, **293-294**, 19-47; (d) D. E. Barry, D. F. Caffrey and T. Gunnlaugsson, *Chem. Soc. Rev.*, 2016, **45**, 3244-3274; (e) Y. Imai, T. Kawai and J. Yuasa, *J. Phys. Chem. A*, 2016, **120**, 4131-4138; (f) S. Engilberge, F. Riobe, S. Di Pietro, L. Lassalle, N. Coquelle, C.-A. Arnaud, D. Pitrat, J.-C. Mulatier, D. Madern, C. Breyton, O. Maury and E. Girard, *Chem. Sci.*, 2017, **8**, 5909-5917; (g) J. Yuasa, T. Nakagawa, Y. Kita, A. Kaito and T. Kawai, *Chem. Commun.*, 2017, **53**, 6748-6751; (h) T. C. Jenks, M. D. Bailey, J. Hovey, S. Fernando, G. Basnayake, M. E. Cross, W. Li and M. J. Allen, *Chem. Sci.*, 2018, **9**, 1273-1278.
6. (a) J.-C. G. Bünzli and S. V. Eliseeva, in *Basics of Lanthanide Photophysics. Lanthanide Luminescence: Photophysical, Analytical and Biological Aspects*, eds. P. Hänninen and H. Härmä, Springer, Heidelberg, 2010, pp. 1-45; (b) L. Di Bari and P. Salvadori, in *Comprehensive Chiroptical Spectroscopy*, 2012, vol. 1, pp. 221-246; (c) J. Feng and H. Zhang, *Chem. Soc. Rev.*, 2013, **42**, 387-410.
7. (a) L. Di Bari, G. Pintacuda and P. Salvadori, *J. Am. Chem. Soc.*, 2000, **122**, 5557-5562; (b) L. Di Bari, G. Pintacuda, P. Salvadori, R. S. Dickins and D. Parker, *J. Am. Chem. Soc.*, 2000, **122**, 9257-9264; (c) L. Di Bari, M. Lelli, G. Pintacuda, G. Pescitelli, F. Marchetti and P. Salvadori, *J. Am. Chem. Soc.*, 2003, **125**, 5549-5558; (d) L. Di Bari and P. Salvadori, *Coord. Chem. Rev.*, 2005, **249**, 2854-2879; (e) L. Di Bari, S. Di Pietro, G. Pescitelli, F. Tur, J. Mansilla and J. M. Saá, *Chem. Eur. J.*, 2010, **16**, 14190-14201; (f) S. Di Pietro, S. L. Piano and L. Di Bari, *Coord. Chem. Rev.*, 2011, **255**, 2810-2820; (g) R. Berardozzi, G. Pescitelli, S. Di Pietro, C. Resta, F. P. Ballistreri, A. Pappalardo, G. A. Tomaselli and L. Di Bari, *Chirality*, 2015, **27**, 857-863; (h) R. Berardozzi and L. Di Bari, *ChemPhysChem*, 2015, **16**, 2868-2875.
8. (a) F. Zinna and L. Di Bari, *Chirality*, 2015, **27**, 1-13; (b) F. Zinna, U. Giovanella and L. Di Bari, *Adv. Mater.*, 2015, **27**, 1791-1795; (c) L. Armelao, D. B. Dell'Amico, L. Bellucci, G. Bottaro, L. Di Bari, L. Labella, F. Marchetti, S. Samaritani and F. Zinna, *Inorg. Chem.*, 2017, **56**, 7010-7018; (d) B. Casanovas, F. Zinna, L. Di Bari, M. S. El Fallah, M. Font-Bardia and R. Vicente, *Dalton Trans.*, 2017, **46**, 6349-6357; (e) M. Leonzio, A. Melchior, G. Faura, M. Tolazzi, F. Zinna, L. Di Bari and F. Piccinelli, *Inorg. Chem.*, 2017, **56**, 4413-4422.
9. F. Zinna, M. Pasini, F. Galeotti, C. Botta, L. Di Bari and U. Giovanella, *Adv. Funct. Mater.*, 2017, **27**, 1603719.
10. (a) J.-C. G. Bünzli and S. V. Eliseeva, *Chem. Sci.*, 2013, **4**, 1939-1949; (b) A. T. Frawley, R. Pal and D. Parker, *Chem. Commun.*, 2016, **52**, 13349-13352; (c) P. Kumar, S. Singh and B. K. Gupta, *Nanoscale*, 2016, **8**, 14297-14340.
11. F. Zinna, PhD thesis, University of Pisa, 2016.
12. J. L. Lunkley, D. Shirotani, K. Yamanari, S. Kaizaki and G. Muller, *Inorg. Chem.*, 2011, **50**, 12724-12732.
13. S. Biju, Y. K. Eom, J.-C. G. Bünzli and H. K. Kim, *J. Mater. Chem. C*, 2013, **1**, 6935-6944.
14. C. Freund, W. Porzio, U. Giovanella, F. Vignali, M. Pasini, S. Destri, A. Mech, S. Di Pietro, L. Di Bari and P. Mineo, *Inorg. Chem.*, 2011, **50**, 5417-5429.
15. (a) T. Harada, Y. Hasegawa, Y. Nakano, M. Fujiki, M. Naito, T. Wada, Y. Inoue and T. Kawai, *J. Alloy. Compd.*, 2009, **488**, 599-602; (b) T. Harada, Y. Nakano, M. Fujiki, M. Naito, T. Kawai and Y. Hasegawa, *Inorg. Chem.*, 2009, **48**, 11242-11250; (c) Y. Kono, K. Nakabayashi, S. Kitamura, M. Shizuma, M. Fujiki and Y. Imai, *RSC Adv.*, 2016, **6**, 40219-40224; (d) Y. Kono, N. Hara, M. Shizuma, M. Fujiki and Y. Imai, *Dalton Trans.*, 2017, **46**, 5170-5174; (e) N. Hara, M. Okazaki, M. Shizuma, S. Marumoto, N. Tajima, M. Fujiki and Y. Imai, *ChemistrySelect*, 2017, **2**, 10317-10322.
16. (a) J. Yuasa, T. Ohno, K. Miyata, H. Tsumatori, Y. Hasegawa and T. Kawai, *J. Am. Chem. Soc.*, 2011, **133**, 9892-9902; (b) Y. Okayasu and J. Yuasa, *Mol. Syst. Des. Eng.*, 2018, **3**, 66-72.
17. T. Hiroyuki, H. Takashi, Y. Junpei, H. Yasuchika and K. Tsuyoshi, *Appl. Phys. Express*, 2011, **4**, 011601.
18. S. Lo Piano, S. Di Pietro and L. Di Bari, *Chem. Commun.*, 2012, **48**, 11996-11998.
19. C. L. Maupin, R. S. Dickins, L. G. Govenlock, C. E. Mathieu, D. Parker, J. A. G. Williams and J. P. Riehl, *J. Phys. Chem. A*, 2000, **104**, 6709-6717.
20. C. Rachel, P. Robert, K. M. Brian, P. Robert, P. David and P. Lars-Olof, *Methods and Appl. Fluoresc.*, 2014, **2**, 024007.
21. (a) E. M. Sánchez-Carnerero, A. R. Agarrabeitia, F. Moreno, B. L. Maroto, G. Muller, M. J. Ortiz and S. de la Moya, *Chem. Eur. J.*, 2015, **21**, 13488-13500; (b) H. Tanaka, Y. Inoue and T. Mori, *ChemPhotoChem*, n/a-n/a.
22. (a) J. Jankowska, J. Paradowska, B. Rakiel and J. Mlynarski, *J. Org. Chem.*, 2007, **72**, 2228-2231; (b) D. Lowicki, A. Bezlada and J. Mlynarski, *Adv. Synth. Catal.*, 2014, **356**, 591-595; (c) M. Bihani and J. C. G. Zhao, *Adv. Synth. Catal.*, 2017, **359**, 534-575; (d) D. Ghorai, V. Müller, H. Keil, D. Stalke, G. Zanoni, B. A. Tkachenko, P. R. Schreiner and L. Ackermann, *Adv. Synth. Catal.*, 2017, **359**, 3137-3141.
23. F. S. Richardson, *Inorg. Chem.*, 1980, **19**, 2806-2812.
24. (a) R. C. Carter, C. E. Miller, R. A. Palmer, P. S. May, D. H. Metcalf and F. S. Richardson, *Chem. Phys. Lett.*, 1986, **131**, 37-43; (b) R. C. Carter, D. H. Metcalf, C. E. Miller, R. A. Palmer, P. S. May, M. F. Reid and F. S. Richardson, *J. Less Common Met.*, 1986, **126**, 303; (c) P. S. May, D. H. Metcalf, F. S. Richardson, R. C. Carter, C. E. Miller and R. A. Palmer, *J. Lumin.*, 1992, **51**, 249-268; (d) S. Petoud, G. Muller, E. G. Moore, J. Xu, J. Sokolnicki, J. P. Riehl, U. N. Le, S. M. Cohen and K. N. Raymond, *J. Am. Chem. Soc.*, 2007, **129**, 77-83; (e) A. D'Aléo, J. Xu, K. Do, G. Muller and K. N. Raymond, *Helv. Chim. Acta*, 2009, **92**, 2439-2460; (f) J. W. Walton, R. Carr, N. H. Evans, A. M. Funk, A. M. Kenwright, D. Parker, D. S. Yufit, M. Botta, S. De Pinto and K. L. Wong, *Inorg. Chem.*, 2012, **51**, 8042-8056.

25. C. J. Barnett, A. F. Drake, R. Kuroda, S. F. Mason and S. Savage, *Chem. Phys. Lett.*, 1980, **70**, 8-10.
26. (a) Y. He, X. Cao, L. A. Nafie and T. B. Freedman, *J. Am. Chem. Soc.*, 2001, **123**, 11320-11321; (b) H. Sato, T. Taniguchi, A. Nakahashi, K. Monde and A. Yamagishi, *Inorg. Chem.*, 2007, **46**, 6755-6766; (c) C. Johannessen and P. W. Thulstrup, *Dalton Trans.*, 2007, 1028-1033; (d) C. Merten, K. Hiller and Y. Xu, *Phys. Chem. Chem. Phys.*, 2012, **14**, 12884-12891; (e) S. R. Domingos, F. Hartl, W. J. Buma and S. Woutersen, *ChemPhysChem*, 2015, **16**, 3363-3373; (f) T. Wu, J. Hudecová, X. Z. You, M. Urbanová and P. Bouř, *Chem. Eur. J.*, 2015, **21**, 5807-5813; (g) R. Berardozzi, E. Badetti, N. A. Carmo dos Santos, K. Wurst, G. Licini, G. Pescitelli, C. Zonta and L. Di Bari, *Chem. Commun.*, 2016, **52**, 8428-8431; (h) L. Arrico, G. Angelici and L. Di Bari, *Org. Biomol. Chem.*, 2016, **15**, 9800-9803.
27. M. Enamullah, A. C. Chamayou, I. Gruber, M. A. Islam, M. Górecki, L. Di Bari, S. Lüdeke, G. Pescitelli and C. Janiak, *in preparation*, 2018.
28. F. Zinna, T. Bruhn, C. A. Guido, J. Ahrens, M. Bröring, L. Di Bari and G. Pescitelli, *Chem. Eur. J.*, 2016, **22**, 16089-16098.